MMC-Based PV Three-Phase System with Distributed MPPT

Simone Barcellona, Marzio Barresi, *Graduate Student Member, IEEE*, Luigi Piegari, *Senior Member, IEEE*

***Abstract*—The use of distributed maximum power point tracking (DMPPT) algorithms is spreading because of their higher efficiency in the case of partial shading. The possibility of integrating photovoltaic (PV) modules in a modular multilevel converter (MMC) connected to the grid has been proposed in recent literature with the advantage of integrating DMPPT algorithms. In the case of partial shading, circulating currents control is necessary to extract the maximum available power and inject symmetric currents in the grid. Novel control strategies for both the ac and dc circulating current components of a three-phase MMC-based PV were proposed and analyzed in this work. Thanks to the presence of a capacitor connected to the dc-side of the MMC, the ac circulating currents could freely be controlled to extract the maximum power from all the PV modules in any irradiance condition while maintaining low power losses. Moreover, in contrast to previous works, instead of measuring the active power of legs and compensating for their imbalance using open-loop control, the power leg mismatches are compensated exploiting the dc loop currents generated through closed loop controls. The effectiveness of the proposed control strategy was proved by simulations performed using MATLAB Simulink®.**

***Index Terms*—distributed MPPT, inhomogeneous irradiance conditions, modular multilevel converter, PV panel.**

I. Introduction

THE need to diversify production sources, reduce the environmental impact, and make energy accessible to all has led to the growing development of renewable energy sources (RESs) such as photovoltaic (PV) plants and wind turbines. Furthermore, the enhancement of the reliability and efficiency of energy storage systems (ESSs) and their cost reduction are improving power system flexibility, and overcoming the obstacles to the variability and intermittency of RESs. In particular, PV plants have been spreading in recent years, with their total global installed capacity reaching 627 GW in 2019 [1].

Different static power converters can be used to interface RESs and ESSs with the electrical network. In particular, PV panels are often connected to the grid through voltage source inverters (VSIs). To extract the maximum available power from a PV panel, a maximum power point tracking (MPPT) algorithm is usually implemented in a dc-dc converter connected between the PV panel and the VSI. Typically, several PV cells are connected in series and/or parallel to form a PV module. Different PV modules can be connected in series to form a string, which increases the total output voltage. Finally, different strings can be connected in parallel to form a PV array, which increases the total available output power of the whole PV system. The most diffused and simplest solution is to connect the whole PV system to the ac grid by means of a single centralized VSI (with or without an intermediate dc-dc converter stage), extracting the maximum power available through a centralized MPPT (CMPPT) algorithm [2]–[4]. However, this solution has several drawbacks. For example, under partial shading conditions, because all the PV modules are connected to the same dc-dc converter, it is not possible to make all the PV panels work at their maximum power point (MPP). Moreover, multiple MPPs can be identified in the equivalent *P*–*V* curve of the array, which cause the MPP tracker to be inefficient [5]–[7]. These drawbacks can be overcome by adopting one of the distributed MPPT (DMPPT) algorithms. Even though several kinds of DMPPT algorithms are reported in the literature, two main categories can be recognized: those for DMPPT at the string level [8] and at the module level [9]–[13]. In this way, each PV string or PV module is connected to a dedicated converter and separately controlled. In both cases, the maximum available power from each string or module can be extracted under any irradiance conditions. Nevertheless, the analyzed solutions do not present high control degrees of freedom. Moreover, high voltages for the grid connection can only be reached by using dedicated transformers. For these reasons, several multilevel converter topologies have been proposed to integrate PV systems. In [14]–[17], a cascaded H-bridge converter was investigated for PV systems. In these applications, the PV strings were interfaced through dedicated dc-dc converters, which were capable of utilizing a distributed MPPT algorithm, and an H-bridge converter. This allowed higher voltage levels and power capabilities to be reached. However, power imbalances due to inhomogeneous irradiance conditions are challenging to manage. In [18], the authors proposed a method to integrate a PV system through the dc-side of a modular multilevel converter (MMC). Although this application is quite simple, it can experience all the drawbacks of the solutions with a centralized inverter. The authors made a significant improvement in [19], [20]. In this case, the PV modules were connected to the capacitors of the submodules (SMs) of the MMC through dc-dc boost converters, allowing

S. Barcellona, M. Barresi and L. Piegari are with the Department of Electronics, Information and Bioengineering, Politecnico di Milano, MI 20133 ITALY (e-mail: simone.barcellona@polimi.it, marzio.barresi@polimi.it, luigi.piegari@polimi.it).

DMPPT. In the case of partial shading conditions, each PV module could work around its theoretical MPP. Thus, high efficiencies could be reached. However, many dc-dc converters were required, preventing this solution from being optimal. A cheaper and more effective solution was proposed in [21]. In this case, the authors proposed a novel structure for interfacing the PV modules directly with the SM capacitors. This solution reduced the total cost of the system because no additional dc-dc converters were needed, but it was more challenging to control it because of the necessity to manage each capacitor voltage at the optimal value provided by the DMPPT. To overcome the power mismatch related to partial shading conditions, the authors in [22] proposed a control strategy based on the generation of both ac and dc circulating currents to balance the power delivered to the grid among the three phases. However, because of the converter topology studied, the three phases of the proposed MMC structure were not entirely decoupled from each other as a result of the absence of a closed path through the dc-side of the converter itself. Therefore, in the case of inhomogeneous irradiance conditions between the arms of one leg of the converter, the ac circulating currents had to reclose in the other two phases, causing greater power losses and higher circulating voltages. Moreover, both the ac and dc circulating current references were generated through open-loop controls by measuring the active power values generated by all the PV modules. Even though this is a simple control strategy, the lack of closed-loop controllers could cause some system instabilities. Another effective control strategy for exploiting the available power of the PV modules using a single-phase modular multilevel converter was proposed in [23]. In this case, for the intrinsic structure of the single-phase converter, its dc-side had to be connected to two capacitors with the middle point accessible to provide a current return path for both the grid and ac circulating currents. This is the main aspect that should be given attention because it can be used even in a three-phase MMC to better manage the power mismatch due to partial shading conditions. Indeed, it could be useful in applications like the one investigated in [22] because it could provide, under specific irradiance conditions, a return path for the ac circulating currents without affecting the other MMC legs and could thus increase the overall system efficiency. Moreover, unlike the method used in [22], the ac current reference is generated through a closed-loop controller that tracks the differences between the PV arm voltages.

In light of the above, this study investigated an innovative control strategy for integrating the PV modules in the SMs of a three-phase MMC with a capacitor on the dc-side. The first main novelty of the present work was the use of the homopolar component of the ac circulating currents to control them freely. This solution has several benefits. A high efficiency can be reached for the DMPPT, along with low power losses, and a better equalization of the ac circulating voltages can be achieved because all three phases of the converter are decoupled. Therefore, in the case of inhomogeneous irradiance conditions between two arms of the same leg, they do not interact with each other. The second main contribution of the present work is related to the generation of the ac and dc circulating current references. Similar to the method used in [23], the ac and dc circulating current references are both generated through closed-loop controllers that track the differences among the PV arm voltages and PV leg voltages, respectively. This study investigated a three-phase MMC to integrate PV modules in a low-voltage network with a rated power of 20 kW. The validity of the proposed control strategy was demonstrated using time-domain simulations performed in a MATLAB Simulink® environment.

The paper is organized as follows. The topology of the proposed three-phase MMC is analyzed in section II. The proposed control strategy is reported in section III. The simulation results that validated the proposed control strategy are presented in section IV. The obtained results are discussed in section V. Finally, some conclusions are drawn in section VI.

II. MMC Three-phase Converter Topology

The proposed converter topology is shown in Fig. 1(a). It consists of three legs, one for each phase. In turn, each leg is composed of two arms connected to each other through a mutually coupled inductor and referred to as upper and lower arms. Each arm contains n series-connected SMs. Each SM comprises series and parallel connections of PV modules directly connected to a capacitor and half-bridge converter. Furthermore, a capacitor is connected to the dc-side of the MMC. Fig. 1(a) shows the electric circuit, where two series capacitors are connected to the dc-side only to simplify the model discussed in the following. In the real system, only one dc capacitor is needed.

Considering Fig. 1(a), the following equations can be derived for each phase, j, of the converter:

$$\begin{cases} v_{up,j} = -v_{g,j} - R_g\left(i_{up,j} - i_{low,j}\right) - L_g \dfrac{d\left(i_{up,j} - i_{low,j}\right)}{dt} + \\ \qquad\qquad - R_{arm} i_{up,j} - L_{arm} \dfrac{di_{up,j}}{dt} - M_{arm} \dfrac{di_{low,j}}{dt} + \dfrac{v_c}{2} \\ v_{low,j} = v_{g,j} + R_g\left(i_{up,j} - i_{low,j}\right) + L_g \dfrac{d\left(i_{up,j} - i_{low,j}\right)}{dt} \\ \qquad\qquad - R_{arm} i_{low,j} - L_{arm} \dfrac{di_{low,j}}{dt} - M_{arm} \dfrac{di_{up,j}}{dt} + \dfrac{v_c}{2} \end{cases} \quad (1)$$

where $v_{up,j}$ and $v_{low,j}$ are the voltages developed by the upper and lower arms of the j-th phase, respectively; v_c is the dc-side voltage; R_{arm} is the arm resistance; L_{arm} is the arm inductance; and M_{arm} is the mutual coupling of the arm inductances. Finally, $i_{up,j}$ and $i_{low,j}$ are the upper and lower arm currents, respectively. Moreover, the voltages developed by the upper and lower arms can be decomposed as follows:

$$\begin{cases} v_{up,j} = -v_{ph,j} + \dfrac{v_{circ,j}}{2} \\ v_{low,j} = v_{ph,j} + \dfrac{v_{circ,j}}{2} \end{cases} \quad (2)$$

where $v_{ph,j}$ is the j-th output phase grid component, while $v_{circ,j}$ is the circulating one. The grid current and circulating current of a generic phase, j, are defined as follows:

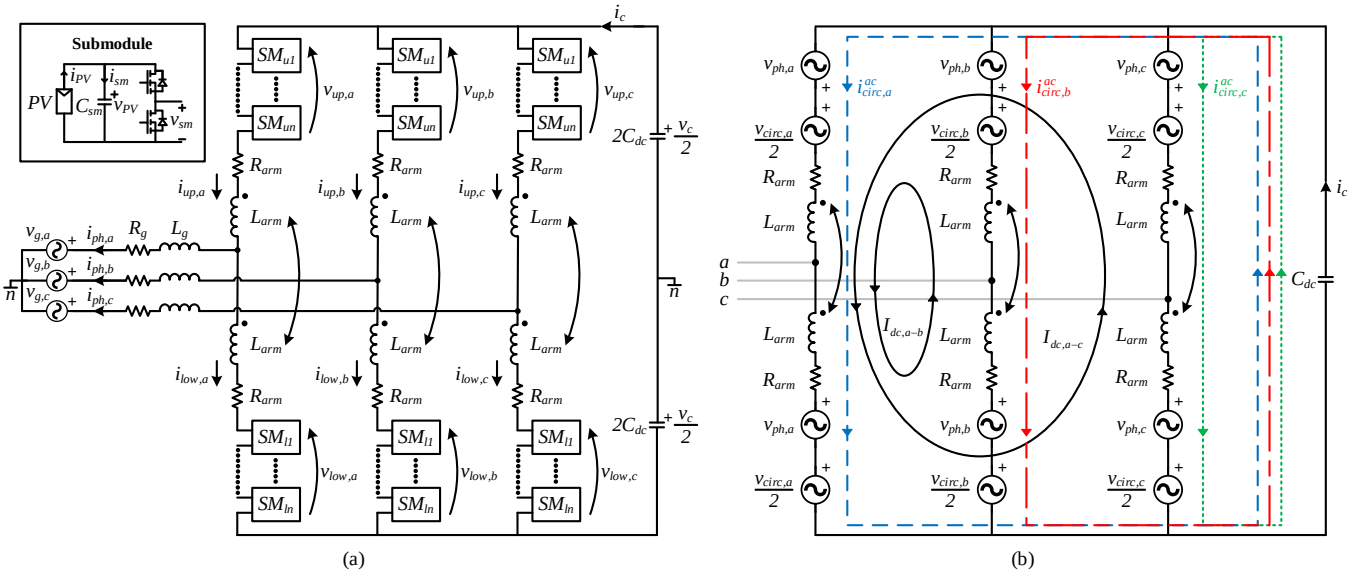

(a) (b)

Fig. 1. Converter topology: a) MMC three-phase with the dc-side capacitor; b) Equivalent circuit of the MMC with the dc-side capacitor.

$$\begin{cases} i_{ph,j} = i_{up,j} - i_{low,j} \\ i_{circ,j} = \dfrac{i_{up,j} + i_{low,j}}{2} \end{cases} . \tag{3}$$

Finally, the related circulating voltage needed to drive the circulating current is represented by the following:

$$v_{circ,j} = -2\left(R_{arm} i_{circ,j} + (L_{arm} + M_{arm}) \frac{di_{circ.j}}{dt} \right) + v_c . \tag{4}$$

The dc-side plays a crucial role in the controller proposed in this work, as will be discussed later. Its voltage is supported by the equivalent capacitor, C_{dc}, and shown as follows:

$$v_c(t) = -\frac{1}{C_{dc}} \int_0^t i_c \, d\tau + v_c(0) \tag{5}$$

where $v_c(0)$ is the initial voltage value of the dc-side capacitor, and i_c is the dc-side current:

$$i_c = i_{circ,a} + i_{circ,b} + i_{circ,c} . \tag{6}$$

The main aim of the proposed control strategy is to deliver the maximum power available from all the PV modules to the ac grid under any irradiance conditions using a DMPPT algorithm. This is achieved by properly controlling both the grid and circulating currents. In particular, the latter are used to manage the power mismatch among the PV modules due to partial shading conditions. Indeed, each PV module, interfaced through the SMs of the MMC, can deliver different power values, leading to possible imbalances between its legs and/or arms. In order to extract the maximum available power and balance the power injected into the grid, proper ac and/or dc components of the circulating currents are controlled through the related circulating voltages. The generated circulating currents and their paths are highlighted in the equivalent circuit of the MMC reported in Fig. 1(b). In all cases, the output phase grid voltages generated by the MMC should only contain the ac positive sequence:

$$v_{ph,j} = v^{ac}_{ph,j} \tag{7}$$

while the circulating voltages must contain an opportune dc voltage component to make the MMC work correctly. This is the homopolar dc voltage, V_{dc}, that charges the capacitor, C_{dc}, to the optimal dc-side voltage. In the case of homogeneous irradiance conditions, the circulating voltages must only have that homopolar dc component. In contrast, in case of inhomogeneous irradiance conditions, the circulating voltages may contain other ac and/or dc components:

$$v_{circ,j} = v^{ac}_{circ,j} + v^{dc}_{circ,j} . \tag{8}$$

We can distinguish two main cases: i. in the case of partial shading conditions among the converter legs, an opportune dc circulating current component is used to balance the power injected into the grid; ii. in the case of partial shading conditions between the arms of the same leg, an opportune ac circulating current component is used to make the DMMPT work properly extracting the maximum power from each SM. The latter, without the presence of the dc-side capacitor, must flow through the other legs of the MMC (even if these other legs are not affected by any inhomogeneous irradiance conditions), in such a way that no active power is exchanged between their arms [22]. Thus, the circulating current will be in quadrature with respect to the other arm voltages by exchanging only reactive power values. In this way, additional losses in both the arm switches and inductors are involved because additional circulating currents flow in the balanced legs of the converter. On the other hand, when a capacitor is connected to the dc-side, the ac circulating current component can flow through this capacitor, without interfering with the other legs of the converter. In this way, each inhomogeneous irradiance condition of the converter legs can be decoupled and controlled separately, with lower losses. Moreover, by opportunely sizing the dc-side capacitor, it could be possible to better equalize the ac circulating voltages. The circuit parameters, including the minimum operational dc voltage, number of SMs, and number of PV modules for each SM, were designed according to the procedure reported in [23].

III. Proposed Control Strategy

The control strategy proposed in [23] for a single-phase system was here extended to a three-phase system. The aim of the control strategy was to inject the maximum power producible by the PV panels under any working condition (i.e., both homogeneous and inhomogeneous solar irradiance) by means of a symmetric system of currents. This was achieved by defining the proper voltage references for both the upper and lower arms of each leg of the converter as follows:

$$\begin{cases} v^*_{up,j} = -v^{ac*}_{ph,j} + \dfrac{v^*_{circ,j}}{2} \\ v^*_{low,j} = v^{ac*}_{ph,j} + \dfrac{v^*_{circ,j}}{2} \end{cases} \quad (9)$$

where $v^{ac*}_{ph,j}$ is the output phase grid voltage reference of the *j*-th phase, and $v^*_{circ,j}$ is the circulating voltage reference of the *j*-th phase, which is defined as follows:

$$v^*_{circ,j} = v^{ac*}_{circ,j} + v^{dc*}_{circ,j}. \quad (10)$$

Both the dc and ac circulating components can, in turn, contain positive, negative, and zero sequences. As previously mentioned, the dc circulating voltages must have the homopolar component to maintain the average value of the dc-side voltage at the best working value. Furthermore, these dc voltages can also contain the positive and/or negative sequences needed to extract the maximum power from each leg in a case of leg unbalance conditions. Finally, the ac circulating voltages can contain all three sequences controlled to extract the maximum power from each arm of each leg in a case of arm unbalanced conditions.

The proposed control strategy, shown in Fig. 2, is organized in three main subsystems: the DMPPT controller, ac/dc power management controller, and converter modulation controller. The DMPPT controller tracks the optimal voltage references for each PV module related to the SMs of the MMC. The power management controller receives these references and generates the related phase grid and circulating voltage references (10). Lastly, the converter modulation controller, after defining the upper and lower arm voltage references according to (9), synthesizes the arm voltage references using the well-known phase disposition pulse width modulation (PD-PWM) with SM balance sorting.

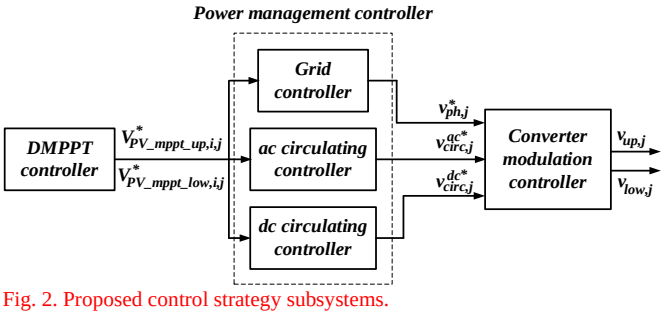

Fig. 2. Proposed control strategy subsystems.

A. DMPPT controller

The DMPPT controller provides reference voltages $V_{PV\_mppt\_up,i,j}$ and $V_{PV\_mppt\_low,i,j}$ for each *i*-th PV module integrated into the SMs, for all the upper and lower arms, to obtain their maximum power under any given solar irradiance condition. In this work, the simplest and most diffused perturb and observe (P&O) method is used. First, currents $i_{PV\_up,i,j}$ and $i_{PV\_low,i,j}$ and voltages $V_{PV\_up,i,j}$ and $V_{PV\_low,i,j}$ of each PV module of all the arms are measured, and then, the power produced is calculated. Second, according to the sign of the ratio between the power and voltage variations (dP/dV), a positive or negative fixed voltage perturbation is applied.

B. Power management controller

The power management controller is the main novelty of the present paper. It can be decomposed into three subsystems: the grid controller, ac circulating controller, and dc circulating controller. These controllers are detailed in the following.

1) Grid controller

The grid controller, depicted in Fig. 3(a), is composed of an outer control loop with a PI regulator that tracks the dc-side voltage, V^*_{dc}, which is defined as the mean value of the voltages of the equivalent dc-side related to the *j*-th leg:

$$V^*_{dc,j} = \frac{\sum_{i=1}^{n_{sm}} V_{PV\_mppt\_up,i,j} + \sum_{i=1}^{n_{sm}} V_{PV\_mppt\_low,i,j}}{2} \quad (11)$$

where n_{sm} is the number of SMs per arm. Therefore, the dc-side voltage is not constant, but changes as a result of the irradiance conditions. This voltage is related to the maximum active power available from all the PV modules. To exchange this power with the grid, the direct component of the current phase reference, $i^*_{ph,d}$, is obtained as the output of the outer PI regulator. On the other hand, the reactive power can be regulated to the desired value using the quadrature component of such a current, $i^*_{ph,q}$. In this case, we assume that zero reactive power is exchanged with the grid to have a unity power factor. Finally, the inner control loop tracks these current components, generating the phase voltage references $v^*_{ph,d}$ and $v^*_{ph,q}$ through two PI regulators. The grid controller is implemented through the Park transformation in a synchronous reference frame locked to the angle θ of the grid voltage, v_g, and leading to the conservation of the amplitudes of the electrical quantities. The synchronization is performed using the phase-locked loop (PLL) control scheme of [24]. Furthermore, the feed-forward terms may be used to make the dynamic response faster. It is worth noting that the inner PI regulators were tuned using the procedure of [25] considering the transfer function between the phase voltages and currents obtainable from (1). The closed loop cut-off frequency was defined equal to 100 Hz. The outer PI regulators were tuned using the trial-and-error method. The PI parameters are reported in Table I.

2) ac circulating controller

The ac circulating controller, shown in Fig. 3(b), is composed of three outer control loops with three PI regulators. The latter track, for each leg, the difference between the upper and lower arms optimal PV reference voltages, provided by the DMMPT

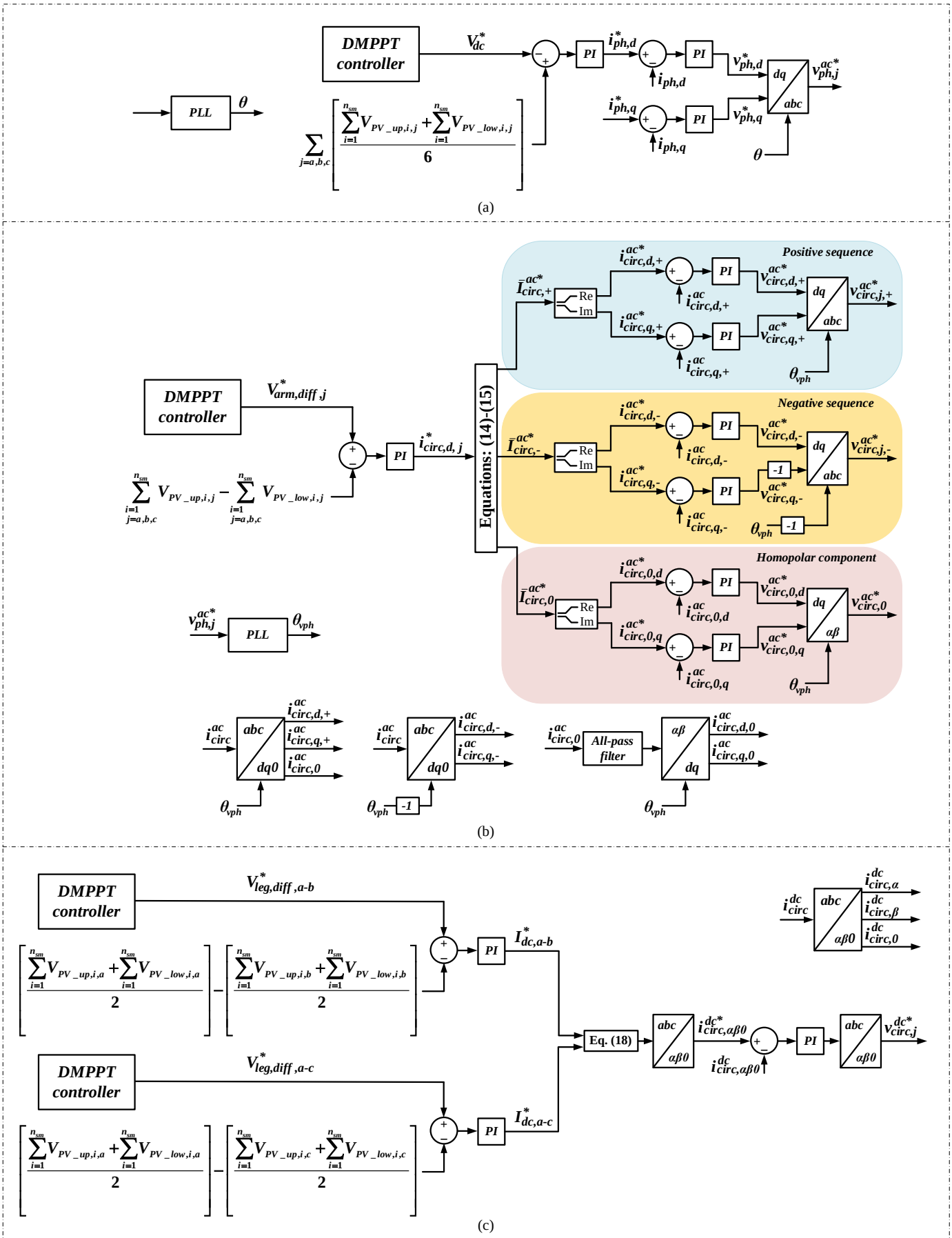

Fig. 3. Control schemes: a) grid controller; b) ac circulating controller; c) dc circulating controller.

controller. They are defined as follows:

$$V^*_{arm,diff,j} = \sum_{\substack{i=1\\ j=a,b,c}}^{n_{sm}} V_{PV\_mppt\_up,i,j} - \sum_{\substack{i=1\\ j=a,b,c}}^{n_{sm}} V_{PV\_mppt\_low,i,j}. \quad (12)$$

This controller is implemented to manage the power mismatch between two arms of the same leg and separately for each leg, using the same strategy reported in [23] for a single-phase MMC. In this way, each arm can operate to its optimal voltage, providing the maximum active power. In contrast to the controller proposed in [23], in order to make a more precise ac circulating controller, it is better to refer to the circulating currents with respect to the output phase grid voltages, $v_{ph,j}$, instead of the grid voltage, v_g, through the angle θ_{vph}. To do this, it is sufficient to add to the Park transformation of the ac circulating controller, the displacement angle, i.e., the phase angle between the output phase grid voltages, $v_{ph,j}$, and the grid voltage v_g. This is achieved, applying another PLL to the generated phase voltage references $v^*_{ph,j}$.

The outputs of the three outer PI regulators are the direct components of the ac circulating current references, $i^{ac*}_{circ,d,j}$. The quadrature components of the circulating currents, $i^{ac*}_{circ,q,j}$, are set equal to zero to prevent the arms from exchanging reactive power.

In the three-phase MMC, the ac circulating currents are the ones that should separately flow in each leg to manage any power mismatch. Because the output phase grid voltages, provided by the grid controller, according to (7), define a fundamental ac positive sequence, although the three ac circulating currents, $i^{ac*}_{circ,d,j}$ can have different amplitudes as a function of the different irradiance conditions per leg, they must be aligned with the related phase voltage (in phase or in opposite phase, depending on the arm power mismatch direction). Therefore, they have a displacement angle of 120° compared to each other. Thus, we can compose a three-phase set of currents whose phasors are expressed as follows (where we assume $i^{ac*}_{circ,q,j} = 0$):

$$\begin{aligned} \bar{I}^{ac*}_{circ,a} &= i^{ac*}_{circ,d,a} \\ \bar{I}^{ac*}_{circ,b} &= i^{ac*}_{circ,d,b}\bar{\alpha}^2 \\ \bar{I}^{ac*}_{circ,c} &= i^{ac*}_{circ,d,c}\bar{\alpha} \end{aligned} \quad (13)$$

where $\bar{\alpha} = e^{j\frac{2}{3}\pi}$.

For this set of currents, all the sequence components (positive, negative, zero) can be present. We obtain the positive, negative, and zero sequences of the circulating current reference according to the Fortescue transformation:

$$\begin{bmatrix} \bar{I}^{ac*}_{circ,+} \\ \bar{I}^{ac*}_{circ,-} \\ \bar{I}^{ac*}_{circ,0} \end{bmatrix} = \frac{1}{3}\begin{bmatrix} 1 & \bar{\alpha} & \bar{\alpha}^2 \\ 1 & \bar{\alpha}^2 & \bar{\alpha} \\ 1 & 1 & 1 \end{bmatrix}\begin{bmatrix} \bar{I}^{ac*}_{circ,a} \\ \bar{I}^{ac*}_{circ,b} \\ \bar{I}^{ac*}_{circ,c} \end{bmatrix}. \quad (14)$$

Considering (13) and (14), we have the following:

$$\begin{aligned} \bar{I}^{ac*}_{circ,+} &= \frac{i^{ac*}_{circ,d,a} + i^{ac*}_{circ,d,b} + i^{ac*}_{circ,d,c}}{3} \\ \bar{I}^{ac*}_{circ,-} &= \frac{i^{ac*}_{circ,d,a} + i^{ac*}_{circ,d,b}\bar{\alpha} + i^{ac*}_{circ,d,c}\bar{\alpha}^2}{3} \\ \bar{I}^{ac*}_{circ,0} &= \frac{i^{ac*}_{circ,d,a} + i^{ac*}_{circ,d,b}\bar{\alpha}^2 + i^{ac*}_{circ,d,c}\bar{\alpha}}{3}. \end{aligned} \quad (15)$$

From (15), we recognize that

$$\bar{I}^{ac*}_{circ,0} = \underline{I}^{ac*}_{circ,-}. \quad (16)$$

The positive and negative sequences are reported in a *dq* reference frame considering the real part as the direct component and the imaginary part as the quadrature one. These are compared with the measured circulating currents, which are transformed using the Park transformation, in both the direct and reverse reference frames. It is worth noting that, for the reverse frame, we obtain a quantity that corresponds to the conjugated negative sequence. In this way, we can track, using four inner control PI regulators, the direct and quadrature components of both the positive and negative circulating current sequences. These PI regulators give the ac direct and quadrature circulating voltage references for both the positive, $v^{ac*}_{circ,d,+}$, $v^{ac*}_{circ,q,+}$, and negative, $v^{ac*}_{circ,d,-}$, $v^{ac*}_{circ,d,-}$ sequences.

The homopolar component of the ac circulating voltage can be obtained by controlling the zero sequence of the ac circulating currents according to (16). To do this, we need two other inner PI regulators for the direct and quadrature components of the single-phase quantity related to the homopolar circulating current. Through the Hilbert transformation, it is possible to obtain these direct and quadrature components. It is worth noting that the inner PI regulators were tuned using the procedure of [25] considering the transfer function between the circulating voltages and currents obtainable from (4). The closed loop cut-off frequency was defined equal to 100 Hz. The outer PI regulators were tuned using the trial-and-error method. The PI parameters are reported in Table I.

3) dc circulating controller

The dc circulating controller, shown in Fig. 3(c), comprises two outer control loops with two PI regulators that track the differences between two pairs of leg PV reference voltages. These are defined as follows:

$$\begin{aligned} V^*_{leg,diff,a-b} &= V^*_{dc,a} - V^*_{dc,b} \\ V^*_{leg,diff,a-c} &= V^*_{dc,a} - V^*_{dc,c}. \end{aligned} \quad (17)$$

This controller is implemented to manage the power mismatch among legs. The outputs of these controllers are the related dc loop currents, $I^*_{dc,a-b}$, $I^*_{dc,a-c}$, between the respective legs, which are defined as follows:

$$\begin{aligned} I^*_{dc,a-b} &= I^{dc*}_{circ,a} - I^{dc*}_{circ,b} \\ I^*_{dc,a-c} &= I^{dc*}_{circ,a} - I^{dc*}_{circ,c}. \end{aligned} \quad (18)$$

$I^{dc*}_{circ,a}$, $I^{dc*}_{circ,b}$, $I^{dc*}_{circ,c}$ are derived from (18), assuming that, under steady-state conditions, the sum of the dc circulating currents is nil. Using the Clarke transformation, the alpha, beta, and

homopolar components of the dc circulating current, $I^{dc*}_{circ,\alpha}, I^{dc*}_{circ,\beta}, I^{dc*}_{circ,0}$, are obtained. Finally, three inner PI regulators, from which the related dc circulation voltage components are generated, track these current references. The PI regulators were tuned exploiting the same methodology of the ac circulating controller. However, in this case, the transfer function of the inner loop can be derived from (1) analyzing the dc circulating current path highlighted in Fig. 1(b). The PI parameters are reported in Table I.

TABLE I
PARAMETERS OF THE PI REGULATORS

Controller	Outer loop		Inner loop	
	k_p	k_i	k_p	k_i
Grid controller	2	30	2.4	88
ac circulating controller	4	1.2	2.5	6.3
dc circulating controller	3	2	2.5	6.3

C. Converter modulation controller

Through the inverse Park transformation, all the output reference signals generated by the previous controllers are provided, in the phase domain, to the converter modulation controller (Fig. 4). The latter synthesizes the former signals using the PD-PWM with SM balance sorting.

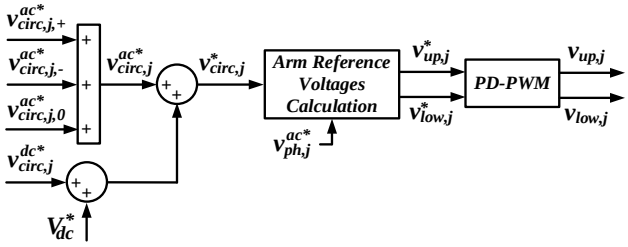

Fig. 4. Converter modulation controller.

IV. Simulation Results

The validity of the proposed control strategy was demonstrated through time-domain simulations performed in MATLAB Simulink®. Starting from homogeneous irradiance conditions, different irradiance conditions were simulated at a specific time. The inhomogeneous conditions were chosen to highlight the effectiveness of the proposed control strategy. Therefore, different partial shading conditions among arms, legs, and even inside the arms were considered. A 20 kW PV-system was connected to a 400 V low-voltage network. The MMC-PV system parameters used in the simulations performed are summarized in Table II. Furthermore, each PV module was modeled according to equation (15) of [23], and the PV temperature was fixed at 25 °C.

TABLE II
MMC-PV SYSTEM PARAMETERS

Parameters	Value	Units
Rated plant power P_{rated}	20	kW
Rated grid phase voltage (rms) $v_{g,i}$	230.9	V
Grid + filter resistance R_g	140	mΩ
Grid + filter inductance L_g	3.9	mH
Arm resistance R_{arm}	5	mΩ
Arm inductance L_{arm}	1	mH
Mutual arm inductance M_{arm}	0.99	mH
SM capacitance C_{sm}	50	mF
dc-side capacitor C_{dc}	5	mF
Number of SMs per arm n_{sm}	12	-
Switching frequency f_s	9	kHz

Each PV module was directly connected to the capacitor of the SM and a P&O MPPT algorithm was implemented for each of them. Finally, the SM sorting based on the theoretical optimal voltage was used [23]. Table III lists the PV module parameters.

TABLE III
PV MODULE PARAMETERS

Parameters	Value	Units
Rated power P_{PV}	42.53	W
Minimum operative irradiance G_{min}	200	W/m^2
Minimum optimal operative PV voltage $V_{mppt,min}$	19.9	V
Number of series PV submodules $n_{PV\ series}$	4	-
Number of parallel PV submodules $n_{PV\ parallel}$	2	-

A. Partial shading conditions between arms of one leg

In this case, inhomogeneous irradiance conditions between the arms of the same leg were analyzed. In this situation, an ac circulating current will flow through the phase affected by unbalanced conditions, making each arm work at its maximum power point. The ac circulating current will not involve the other two converter legs, but it will flow through the dc-side capacitor. Initially, all the PV modules are subjected to the maximum irradiance value, i.e., 1000 W/m^2. Then, after 5 s, the irradiance of the PV modules embedded in the lower arm of phase *a* decreased to 390 W/m^2. The irradiance of the SM embedded in the arms of legs *b* and *c* decreased to 700 W/m^2, guaranteeing that the power available is always the same for the three legs and, thus, no dc circulating current is needed. Table IV reports the power values generated in the arms. The simulation results are reported in Fig. 5. In this scenario, it is possible to recognize the basic principle of the proposed control strategy. During the first 5 s, after a short transient, the arm voltages reach, as mean values, their theoretical optimal values. In this case, all the converter PV modules are irradiated in the same way, and therefore no circulating currents are needed. After 5 s, an ac circulating current is needed for leg *a* to ensure that its arms work at the MPP. This current, because it must not affect the other two converter legs, will flow through the dc-side capacitor. The dc and ac (50 Hz) circulating currents and the capacitor current were extrapolated through the Fast Fourier Transform, and they are reported in Fig. 5(d). Moreover, no dc circulating currents are needed because the power values delivered by each converter leg are equal each other (Fig. 5(e)). Therefore, no dc circulating current is needed, and the power delivered to the grid turns out to be constant (Fig. 5(f)). The efficiency reached using the proposed DMPPT controller was equal to 99.9%.

TABLE IV
GENERATED ARM POWER VALUES IN SCENARIO A

Leg	Upper arm		Lower arm	
	P (kW)			
	t = 0-5 s	t = 5-10 s	t = 0-5 s	t = 5-10 s
Leg *a*	4.083	4.083	4.083	1.505
Leg *b*	4.083	2.794	4.083	2.794
Leg c	4.083	2.794	4.083	2.794

B. Partial shading conditions between legs

In this case, inhomogeneous irradiance conditions among the converter legs were analyzed. Initially, all the PV modules were subjected to the maximum irradiance value, i.e., 1000 W/m^2. Therefore, no circulating components were needed. Then, after

5 s, the irradiance of the PV modules in the converter leg of phase *a* was decreased to 600 W/m^2. The irradiance of the PV modules in the converter leg of phase *b* decreased to 200 W/m^2 and the irradiance of the PV modules in the converter leg of phase *c* decreased to 800 W/m^2. Table V reports the power values generated by the arms. The simulation results are reported in Fig. 6. In this scenario, after 5 s, three dc circulating components are generated to balance the power among the converter legs. In Fig. 6(d), the circulating current components, analyzed through the Fast Fourier Transform, are reported. The amplitudes of the three dc circulating currents depend on the power mismatch among the phases. Because the power values produced by legs *a* and *c* are greater than that of leg *b*, they will transfer power to the latter. The dc circulating current related to leg *c* is the highest because it produces the highest power. Moreover, no ac circulating currents are needed because the arms of the same converter leg are irradiated homogeneously (Fig. 6(d)) and power produced by the arms of the same leg are equal each other (Fig. 6(e)). Finally, no unbalanced currents flow through the grid, and the generated power remains balanced (Fig. 6(f)), leading a DMPTT controller efficiency of 99.9%.

TABLE V
GENERATED ARM POWER VALUES IN SCENARIO B

Leg	Upper arm		Lower arm	
	P (kW)			
	t = 0-5 s	t = 5-10 s	t = 0-5 s	t = 5-10 s
Leg *a*	4.083	2.371	4.083	2.371
Leg *b*	4.083	0.734	4.083	0.734
Leg c	4.083	3.220	4.083	3.220

C. Partial shading conditions between arms and legs

In this case, inhomogeneous irradiance conditions among the arms and legs of the converter were analyzed. Initially, all the PV modules were subjected to the maximum irradiance value, i.e., 1000 W/m^2. Therefore, no circulating components were needed. Then, after 5 s, the irradiance of the PV modules changed in different ways between the converter arms, keeping the same solar irradiance for the PV modules belonging to the same arm. The generated power results are reported in Table VI. The simulation results are reported in Fig. 7. In this scenario, after 5 s, both the ac and dc circulating components are generated to balance the power values due to the power mismatch among the converter legs and arms (Fig. 7(e)). The ac circulating components are used to extract the maximum power among the arms, and their sum flows through the dc-side capacitor. Instead, the dc circulating components balance the power among the legs.

TABLE VI
GENERATED ARM POWER VALUES IN SCENARIO C

Leg	Upper arm		Lower arm	
	P (kW)			
	t = 0-5 s	t = 5-10 s	t = 0-5 s	t = 5-10 s
Leg *a*	4.083	3.612	4.083	2.165
Leg *b*	4.083	1.271	4.083	1.645
Leg c	4.083	2.740	4.083	3.376

D. Partial shading conditions for one arm of the converter

In this case, inhomogeneous irradiance conditions for one arm of the converter were analyzed. Initially, all the PV modules were subjected to the maximum amount of irradiance, i.e., 1000 W/m^2. Then, after 5 s, the irradiance of the twelve PV modules embedded in the upper arm of phase *a* changed to 0.4-1-1-0.3-1-1-0.9-1-1-0.8-1-1 kW/m^2, while the irradiance of all the SMs embedded in the other converter arms decreased to 500 W/m^2. Table VII reports the power values generated in the arms. This condition involved a power mismatch between the arms of leg *a* and between the three legs. Therefore, both ac and dc circulating currents were needed to ensure that each arm worked at its maximum power point and at the same time injected balanced currents into the grid.

The simulation results are reported in Fig. 8. The same conclusions for scenario *C* can be derived from the voltages, currents, and grid power behavior. Moreover, looking at Fig. 9, the effectiveness of the proposed control strategy is worth noting. Indeed, even under extremely unbalanced irradiance conditions, each PV module could work at its maximum power point. As a result, the efficiency reached using the proposed DMPPT controller was equal to 99.9% in this scenario.

TABLE VII
GENERATED ARM POWER VALUES IN SCENARIO D

Leg	Upper arm		Lower arm	
	P (kW)			
	t = 0-5 s	t = 5-10 s	t = 0-5 s	t = 5-10 s
Leg *a*	4.083	3.517	4.083	1.952
Leg *b*	4.083	1.952	4.083	1.952
Leg c	4.083	1.952	4.083	1.952

V. DISCUSSION

The simulation results reported in the previous section showed the robustness of the proposed MMC-based PV three-phase system under any solar irradiance condition. Indeed, in all the analyzed scenarios, each PV module produced the maximum available power because the proposed DMPPT achieved high efficiency.

Scenario A showed the first main aspect of the proposed topology and control strategy. In this case, the unbalanced irradiance conditions between two arms of leg *a* did not affect the other two balanced phases of the MMC. Indeed, the generated ac circulating current of the affected phase flowed in the dc-side capacitor. With respect to the work presented in [22], where the dc-side capacitor was not present, under the same condition, the ac circulating current was constrained to reclose in the other two legs, even if these other legs were not affected by any inhomogeneous irradiance conditions. This involved additional losses in legs *b* and *c* and higher circulating voltages. In fact, although it is outside of the scope of the present work, it is possible to properly design the dc-side capacitor to optimize the power losses and equalize the circulating voltages among the legs. Scenario B showed the second main feature of the proposed control strategy. In this situation, unbalanced irradiance conditions among the converter legs were analyzed. Because the arms belonging to the same leg were equally irradiated, only dc circulating currents were generated. In contrast to the method used in [22], the current references were generated through closed control loops that tracked the differences between two pairs of leg PV reference voltages according to (17). Even though this method is slightly more complex, it increases the system stability, and the response of the system is not affected by disturbances.

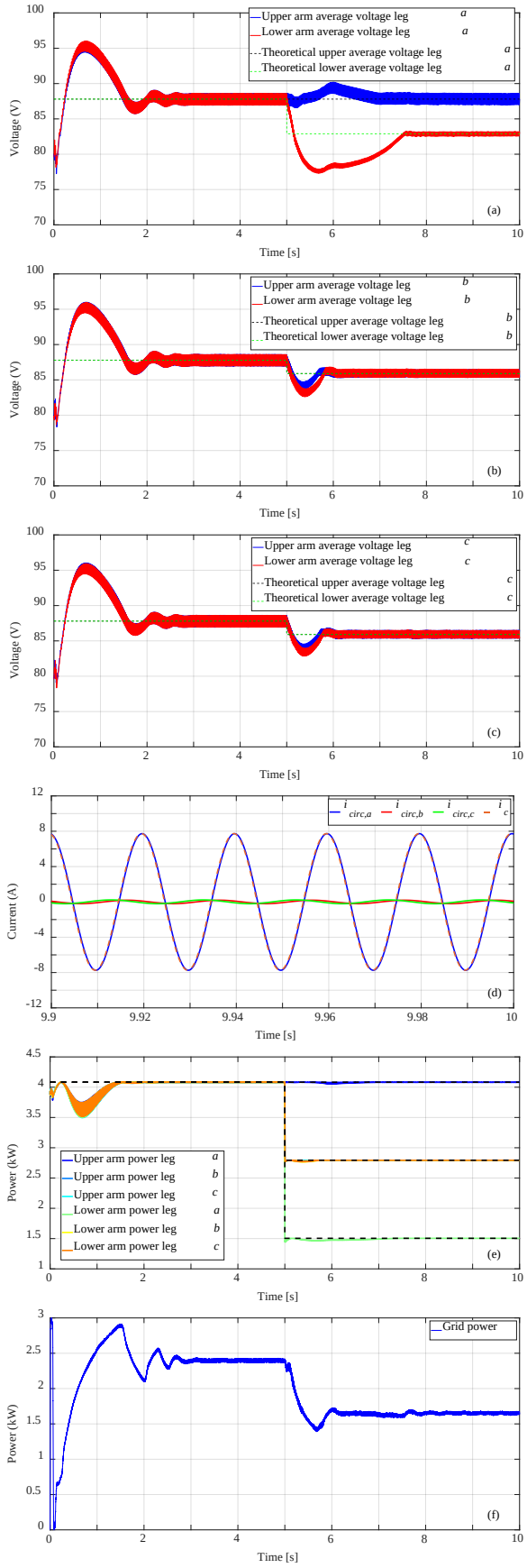

Fig. 5. Partial shading conditions between arms of one leg: a), b), and c) upper and lower average arm voltages for legs a, b, and c respectively; d) dc component and first harmonic of circulating currents; e) generated arm powers. The dashed lines represent the maximum available power; f) grid power.

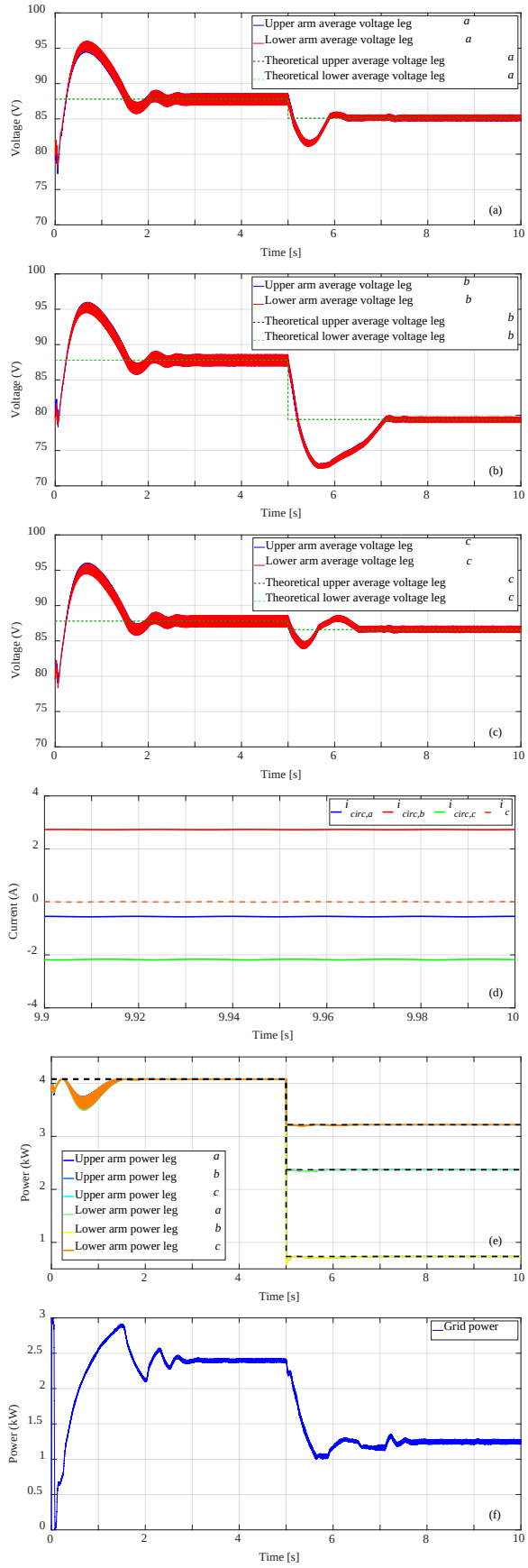

Fig. 6. Partial shading conditions between converter legs: a), b), and c) upper and lower average arm voltages for legs a, b, and c, respectively; d) dc component and first harmonic of circulating currents; e) generated arm powers. The dashed lines represent the maximum available power; f) grid power.

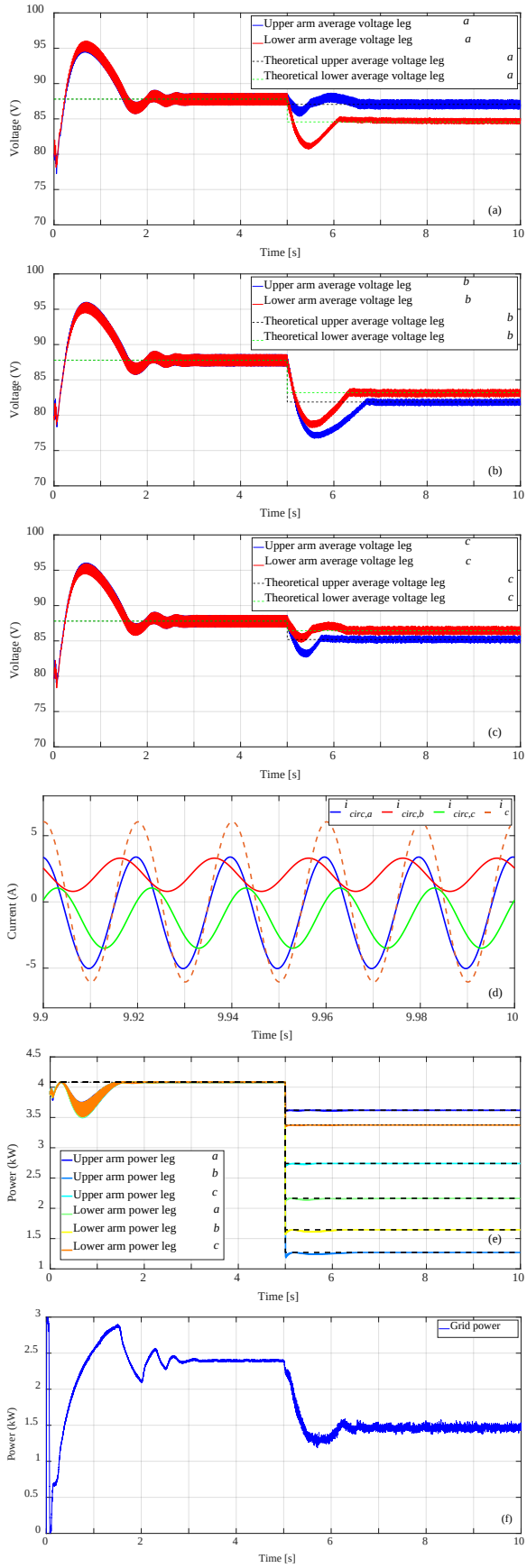

Fig. 7. Partial shading conditions between converter arms and legs: a), b), and c) upper and lower average arm voltages for legs a, b, and c, respectively; d) dc component and first harmonic of circulating currents; e) generated arm powers. The dashed lines represent the maximum available power; f) grid power.

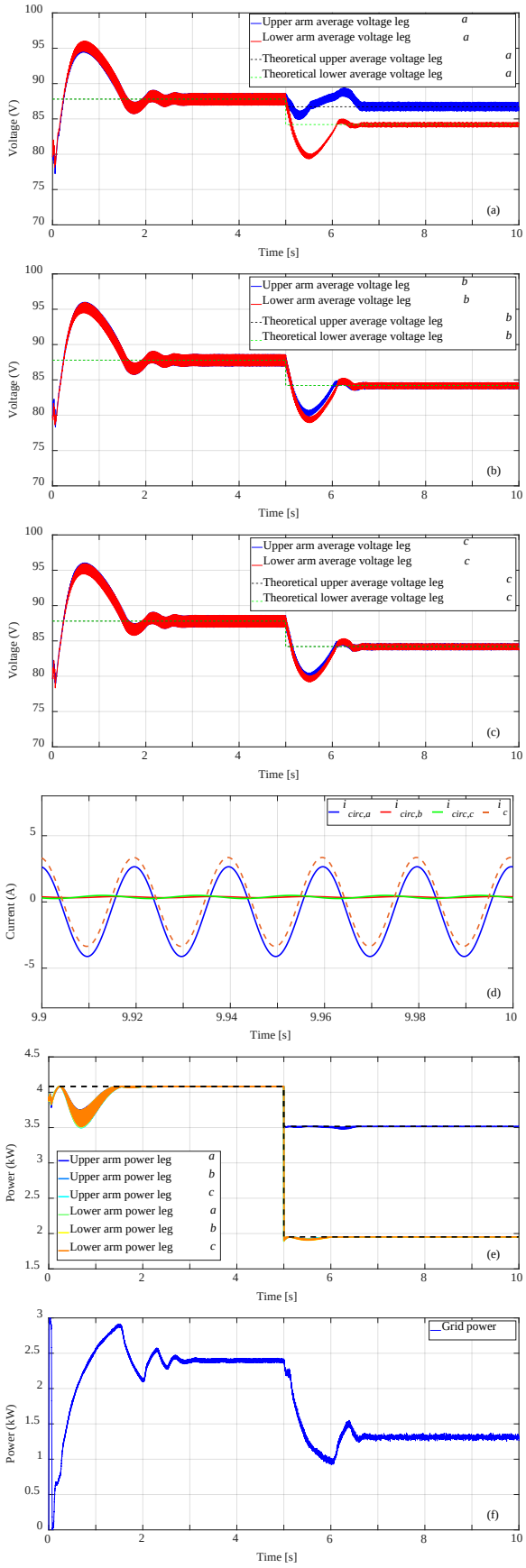

Fig. 8. Partial shading conditions for one arm of the converter: a), b), and c) upper and lower average arm voltages for legs a, b, and c, respectively; d) dc component and first harmonic of circulating currents; e) generated arm powers. The dashed lines represent the maximum available power; f) grid power.

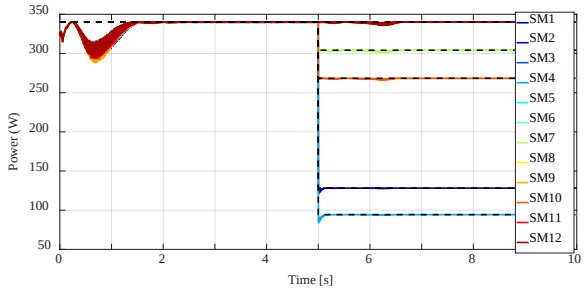

Fig. 9. Generated PV module powers. The dashed lines represent the maximum available power.

Finally, in scenarios C and D, unbalanced irradiance conditions among arms and legs of the converter were analyzed, showing the effectiveness of the entire system in which both ac and dc circulating currents are present. In more detail, scenario D showed a power mismatch even among the SMs of one arm of the MMC.

VI. Conclusions

In this study, a novel control strategy for an MMC-based PV three-phase system was proposed and analyzed.

The first main novelty of the present work is the use of the dc-side of the MMC to freely control the homopolar component of the ac circulating currents in a case of arm power mismatch. Through the proposed control strategy, the ac circulating currents, in general, can flow in the dc-side. In a case of an arm power mismatch in only one leg, the ac circulating current of the leg affected by the mismatch can reclose in the dc-side, resulting in low power losses.

The second main contribution of the present work is the dc circulating current control strategy. Instead of measuring the active power mismatch among the legs as done in [22], in this case, similarly to the ac circulating controller, the differences between the optimal reference voltages for two different pairs of legs given by the DMPPT are tracked. Lastly, the generated dc loop circulating currents among the legs are controlled.
Finally, the effectiveness of the proposed control strategy was proved by means of numerical simulation results. Under both homogeneous and very inhomogeneous solar irradiance conditions, the DMPPT efficiency was always 99.9%, while keeping the currents injected into the grid balanced.

References

[1] Renewable Energy Policy Network for the 21st Century, "Renewables 2020 global status report,"2020.

[2] M. Kasper, D. Bortis and J. W. Kolar, "Classification and Comparative Evaluation of PV Panel-Integrated DC–DC Converter Concepts," in *IEEE Transactions on Power Electronics*, vol. 29, no. 5, pp. 2511-2526, May 2014, doi: 10.1109/TPEL.2013.2273399.

[3] L. Bowtell and A. Ahfock, "Direct current offset controller for transformerless single-phase photovoltaic grid-connected inverters," in *IET Renewable Power Generation*, vol. 4, no. 5, pp. 428-437, September 2010, doi: 10.1049/iet-rpg.2009.0043.

[4] W. Libo, Z. Zhengming and L. Jianzheng, "A Single-Stage Three-Phase Grid-Connected Photovoltaic System With Modified MPPT Method and Reactive Power Compensation," in *IEEE Transactions on Energy Conversion*, vol. 22, no. 4, pp. 881-886, Dec. 2007, doi: 10.1109/TEC.2007.895461.

[5] K. Chen, S. Tian, Y. Cheng and L. Bai, "An Improved MPPT Controller for Photovoltaic System Under Partial Shading Condition," in *IEEE Transactions on Sustainable Energy*, vol. 5, no. 3, pp. 978-985, July 2014, doi: 10.1109/TSTE.2014.2315653.

[6] I. R. Balasubramanian, S. I. Ganesan and N. Chilakapati, "Impact of partial shading on the output power of PV systems under partial shading conditions," in *IET Power Electronics*, vol. 7, no. 3, pp. 657-666, March 2014, doi: 10.1049/iet-pel.2013.0143.

[7] A. Bidram, A. Davoudi and R. S. Balog, "Control and Circuit Techniques to Mitigate Partial Shading Effects in Photovoltaic Arrays," in *IEEE Journal of Photovoltaics*, vol. 2, no. 4, pp. 532-546, Oct. 2012, doi: 10.1109/JPHOTOV.2012.2202879.

[8] H. Keyhani and H. A. Toliyat, "Single-Stage Multistring PV Inverter With an Isolated High-Frequency Link and Soft-Switching Operation," in *IEEE Transactions on Power Electronics*, vol. 29, no. 8, pp. 3919-3929, Aug. 2014, doi: 10.1109/TPEL.2013.2288361.

[9] Abdalla, I.; Corda, J.; Zhang, Z. Multilevel DC-link inverter and control algorithm to overcome the PV partial shading. IEEE Trans. Power Electron., 2013, Volume 28, no. 1, pp. 14–18.

[10] Hu, Y., Wu, J., Cao, W., et al. Ultra-high step-up DC–DC converter for distributed generation by three degrees of freedom (3DoF) approach. IEEE Trans. Power Electron., 2016, 31, (7), pp. 4930–4941.

[11] M. O. Badawy, S. M. Bose and Y. Sozer, "A Novel Differential Power Processing Architecture for a Partially Shaded PV String Using Distributed Control," in IEEE Transactions on Industry Applications, vol. 57, no. 2, pp. 1725-1735, March-April 2021, doi: 10.1109/TIA.2020.3046430.

[12] S. R. Pendem, S. Mikkili and P. K. Bonthagorla, "PV Distributed-MPP Tracking: Total-Cross-Tied Configuration of String-Integrated-Converters to Extract the Maximum Power Under Various PSCs," in IEEE Systems Journal, vol. 14, no. 1, pp. 1046-1057, March 2020, doi: 10.1109/JSYST.2019.2919768.

[13] R. López-Erauskin, A. González, G. Petrone, G. Spagnuolo and J. Gyselinck, "Multi-Variable Perturb and Observe Algorithm for Grid-Tied PV Systems With Joint Central and Distributed MPPT Configuration," in IEEE Transactions on Sustainable Energy, vol. 12, no. 1, pp. 360-367, Jan. 2021, doi: 10.1109/TSTE.2020.2996089.

[14] B. Xiao, L. Hang, J. Mei, C. Riley, L. M. Tolbert and B. Ozpineci, "Modular Cascaded H-Bridge Multilevel PV Inverter With Distributed MPPT for Grid-Connected Applications," in *IEEE Transactions on Industry Applications*, vol. 51, no. 2, pp. 1722-1731, March-April 2015, doi: 10.1109/TIA.2014.2354396.

[15] D. Iannuzzi, L. Piegari and P. Tricoli, "A novel PV-modular multilevel converter for building integrated photovoltaics," *2013 Eighth International Conference and Exhibition on Ecological Vehicles and Renewable Energies (EVER)*, Monte Carlo, 2013, pp. 1-7, doi: 10.1109/EVER.2013.6521620.

[16] Y. Yu, G. Konstantinou, B. Hredzak and V. G. Agelidis, "Power Balance Optimization of Cascaded H-Bridge Multilevel Converters for Large-Scale Photovoltaic Integration," in *IEEE Transactions on Power Electronics*, vol. 31, no. 2, pp. 1108-1120, Feb. 2016, doi: 10.1109/TPEL.2015.2407884.

[17] Y. Yu, G. Konstantinou, C. D. Townsend and V. G. Agelidis, "Comparison of zero-sequence injection methods in cascaded H-bridge multilevel converters for large-scale photovoltaic integration," in *IET Renewable Power Generation*, vol. 11, no. 5, pp. 603-613, 12 4 2017, doi: 10.1049/iet-rpg.2016.0621.

[18] G. Ramya and R. Ramaprabha, "Design methodology of P-Res controllers with harmonic compensation technique for modular multilevel converter fed from partially shaded PV array," *2015 IEEE 11th International Conference on Power Electronics and Drive Systems*, Sydney, NSW, 2015, pp. 330-335, doi: 10.1109/PEDS.2015.7203503.

[19] J. Echeverría, S. Kouro, M. Pérez and H. Abu-rub, "Multi-modular cascaded DC-DC converter for HVDC grid connection of large-scale photovoltaic power systems," *IECON 2013 - 39th Annual Conference of the IEEE Industrial Electronics Society*, Vienna, 2013, pp. 6999-7005, doi: 10.1109/IECON.2013.6700293.

[20] S. Rivera, B. Wu, R. Lizana, S. Kouro, M. Perez and J. Rodriguez, "Modular multilevel converter for large-scale multistring photovoltaic energy conversion system," *2013 IEEE Energy Conversion Congress and Exposition*, Denver, CO, 2013, pp. 1941-1946, doi: 10.1109/ECCE.2013.6646945.

[21] F. Rong, X. Gong and S. Huang, "A Novel Grid-Connected PV System Based on MMC to Get the Maximum Power Under Partial Shading Conditions," in *IEEE Transactions on Power Electronics*, vol. 32, no. 6, pp. 4320-4333, June 2017, doi: 10.1109/TPEL.2016.2594078.

[22] H. Bayat and A. Yazdani, "A Power Mismatch Elimination Strategy for an MMC-Based Photovoltaic System," in *IEEE Transactions on Energy Conversion*, vol. 33, no. 3, pp. 1519-1528, Sept. 2018, doi: 10.1109/TEC.2018.2819982.

[23] Barcellona, S.; Barresi, M.; Piegari, L. MMC-Based PV Single-Phase System with Distributed MPPT. *Energies* 2020, *13*, 3964.

[24] F. Blaabjerg, R. Teodorescu, M. Liserre and A. V. Timbus, "Overview of Control and Grid Synchronization for Distributed Power Generation Systems," in IEEE Transactions on Industrial Electronics, vol. 53, no. 5, pp. 1398-1409, Oct. 2006, doi: 10.1109/TIE.2006.881997.

[25] L. Harnefors and H. -. Nee, "Model-based current control of AC machines using the internal model control method," in *IEEE Transactions on Industry Applications*, vol. 34, no. 1, pp. 133-141, Jan.-Feb. 1998, doi: 10.1109/28.658735.